

Research Article

Laboratory Investigation

Acceleration of tumor growth due to dysfunction in M1 macrophages and enhanced angiogenesis in an animal model of autoimmune disease

Tomoyuki Kondo¹, Takaaki Tsunematsu¹, Akiko Yamada¹, Rieko Arakaki¹,
Masako Saito¹, Kunihiro Otsuka¹, Satoko Kujiraoka¹, Aya Ushio¹, Mie Kurosawa¹,
Yasusei Kudo¹, and Naozumi Ishimaru¹

¹Department of Oral Molecular Pathology, Institute of Biomedical Sciences,
Tokushima University Graduate School, Tokushima, Japan

Correspondence: Professor N Ishimaru, D.D.S., Ph.D, Department of Oral
Molecular Pathology, Institute of Biomedical Sciences, Tokushima University
Graduate School 3-18-15 Kuramoto-cho, Tokushima 7708504, Japan.

E-mail: ishimaru.n@tokushima-u.ac.jp

Abstract

Both autoimmunity and tumor immunity are immune responses against self-tissues or cells. However, the precise similarity or difference between them remains unclear. In this study, to understand a novel mechanism of tumor immunity, we performed transplantation experiments with a murine autoimmune model, C57BL/6J (B6)/*lpr* mice. A melanoma cell line, B16F10 cells, or granulocyte macrophage colony-stimulating factor- overexpressing B16F10 (B16F10/mGM) cells were transplanted into B6 or B6/*lpr* mice. Tumor growth by transplanted B16F10/mGM cells was significantly accelerated in B6/*lpr* mice compared with that in B6 mice. The accumulation of M1 macrophages in the tumor tissues of B6/*lpr* recipient mice was significantly lower compared with that in the control mice. *In vitro* co-culture experiment showed that impaired differentiation into M1 macrophages was observed in B6/*lpr* mice. The number of tumor vessels and vascular endothelial growth factor (VEGF) expression were also significantly enhanced in the tumor tissues of B6/*lpr* mice compared with those in the B6 mice. Moreover, VEGF expression was correlated with the increased expression of hypoxia-inducible factor-1 α in the tumor tissues of B6/*lpr* mice. These results suggest that dysfunctional tumor immunity and enhanced angiogenesis in autoimmunity influence tumor growth.

Introduction

Anti-tumor immune responses are operated during each step of tumor progression.^{1,2} However, in most cases, the anti-immune responses are suppressed and attenuated by

tumors and tumor microenvironments, thus the immune responses are ineffective and insufficient.^{1,2} Various types of immune cells are associated with tumor immunity, including cytotoxic T cells, macrophages, dendritic cells, and regulatory T cells, which contribute to the survival, death, growth, and differentiation of the tumor cells via complex mechanisms.³ In particular, a recent study showed that tumor-associated macrophages (TAMs) play key roles in the survival, invasion, motility, and intravasation of tumor cells.⁴

Macrophages have highly diverse functions in different organs, local environments, and in response to antigens.^{5,6} It is well known that there are two classes of macrophages: (i) activated (M1) macrophages which respond to tumor necrosis factor (TNF)- α , interferon (IFN)- γ , and ligands/toll-like receptor 4; and (ii) alternately activated (M2) macrophages which respond to interleukin (IL)-4 and IL-13.⁷ It has also been reported that TAMs are polarized into the two classes of tumor-killing (M1) and tumor-promoting (M2) macrophages.⁸

The autoimmune response is known to be exceptionally complicated.^{9,10} Autoimmune diseases are caused by multiple factors, such as dysfunctional immune cells, dysregulation of the immune system, genetic factors, infections, and environmental factors.^{9,11,12} Several studies have shown that macrophages play major roles in the onset or development of autoimmunity.^{13,14} In particular, activated M1 macrophages contribute to the enhancement or acceleration of experimental autoimmune encephalomyelitis and Sjögren's syndrome-like lesions in animal models.^{15,16} Therefore, during autoimmunity, we hypothesized that M1 macrophages

may have an anti-tumor role in tumor immunity. In addition, recent studies of the relationship between autoimmunity and tumor immunity demonstrate that the incidence rate of some malignant tumors, such as hematological tumors, lung cancer, and thyroid cancer, is epidemiologically higher in the patients with systemic lupus erythematosus (SLE) or rheumatoid arthritis (RA) than that in healthy controls.¹⁷⁻²⁰ However, the precise relationship between autoimmunity and tumor immunity remains unclear.

In this study, to investigate a novel regulatory mechanism for tumor immunity mediated by macrophages, we performed transplantation experiments using a murine autoimmune model to analyze the development of tumors in an environment with autoimmunity.

MATERIALS AND METHODS

Mice and Tumor Transplantation

C57BL/6J (B6) and B6-*Fas^{lpr}*/J (B6/*lpr*) mice were purchased from the Japan SLC Laboratory (Shizuoka, Japan). Male mice were reared in our specific pathogen-free mouse colony, where food and water provided ad libitum. B16F1, B16F10, B16F10/mGM melanoma cells, and 3LL cells were supplied by RIKEN (No. RCB2649, RCB2630, and RCB1158) and National Institutes of Biomedical Innovation, Health and Nutrition (No. JCRB1348). The cells were maintained in DMEM (Wako Pure Chemical Industries, Ltd., Osaka, Japan) with 10% fetal bovine serum (FBS). Next, 10⁶ cells in 100 μ l PBS were injected subcutaneously into B6 or B6/*lpr* mice. At 3 weeks after injection, X-ray computed tomography (CT) images were captured using SkyScan 1176

system (Bruker microCT, Kontich, Belgium) and tumor volume was analyzed by CTAn (Bruker microCT), before analyzing the size and weight of tumors. In addition, the removed tumor tissues were used in further experiments. The survival ratio was calculated using the Kaplan–Meier method. This study was conducted in accordance with the “Fundamental Guidelines for the Proper Conduct of Animal Experiments and Related Activities in Academic Research Institutions” under the jurisdiction of the Ministry of Education, Culture, Sports, Science and Technology of the Japanese Government. The study protocols were approved by the Committee on Animal Experiments of Tokushima University (Permit Number: toku-15011).

Flow Cytometric Analysis

Infiltrating immune cells in tumor tissues were collected by enzymatic digestion using collagenase type I (Wako Pure Chemical Industries) and dispase (EIDIA Co., Ltd., Tokyo, Japan). The suspended cells were analyzed using the following monoclonal antibodies (mAbs): FITC-, PE-, APC-, APC-Cy7-, PE-Cy7-, APC-eFluor780-, PerCP-Cy5.5, eFluor 450- or Brilliant Violet 420-conjugated anti-mouse CD3, CD19, NK1.1, CD45.2, CD11b, CD11c, F4/80, and CD206 (eBioscience, Inc., San Diego, CA). An EC800 analyzer (Sony Corporation, Tokyo, Japan) was employed to determine the cell populations, and the data were processed using EC800 v1.3.6 FACS analysis software (Sony Corporation). Cell numbers were determined with a Coulter particle counter (Beckman Coulter, Inc., Brea, CA).

Histopathological and Immunofluorescence Analysis

Tumor tissues were removed from mice, fixed with 10% phosphate-buffered formaldehyde (pH 7.2) and prepared for histological examination. Sections were stained with hematoxylin and eosin (H&E). For the immunofluorescence analysis, paraffin-embedded sections were stained with anti-Ki67 (Novus Biologicals, LLC, Littleton, CO, USA), anti-CD31 (Abcam plc, Cambridge, UK), anti-VEGF-A (Abcam plc), anti-pimonidazole (Hypoxypore, Inc., Burlington, MA), and anti-HIF-1 α (Novus Biologicals, LLC, Littleton, CO) mAb, before applying an Alexa-555-conjugated secondary antibody. The nuclei were stained with 4',6-diamidino-2-phenylindole (DAPI) (Life Technologies, Carlsbad, CA). A HypoxyporeTM-1 Omni kit (Hypoxypore, Inc.) was used to detect hypoxia in tumor cells. Briefly, 1.5 mg pimonidazol was injected intravenously into mice with transplanted tumors. The tumor tissues were fixed at 30 min after injecting pimonidazol and then the hypoxic cells were then detected by immunofluorescence analysis. The images were acquired using an observer z1 (Carl Zeiss, Oberkochen, Germany) and analyzed with axio vision se64 (Carl Zeiss).

Enzyme-Linked Immunosorbent Assay (ELISA)

The concentration of VEGF in tumor tissues was measured using a mouse VEGF ELISA kit (RayBiotech, Inc., Norcross, GE). Diluted samples or standard recombinant VEGF were added to 96-well flat-bottomed plates precoated with capture antibodies. After washing the plates, biotinylated antibodies were added and the wells were

incubated with streptavidin conjugated horseradish peroxidase (HRP). Tetramethylbenzidine solution was added to each well as the substrate. The optimal density at 450 nm was measured using a microplate reader (model 680; Bio-Rad Laboratories, Inc., Hercules, CA).

Real-Time RT-PCR

Total RNA was isolated from removed tumor tissues using TRI Reagent® (Molecular Research Center, Inc., Cincinnati, OH). Total RNA was reverse transcribed using a PrimeScript® RT reagent kit (Takara Bio Inc., Shiga, Japan) and the cDNA obtained was used as the PCR template. Transcript levels were determined using a 7300 Real-time PCR System (Life Technologies) with SYBR Premix Ex Taq (Takara Bio Inc.). The primer sequences used are shown in Supplementary Table S1. The relative mRNA expression level of each transcript was normalized against that of β -actin mRNA.

Co-culture Analysis

1×10^5 B16F10/mGM cells were seeded into 24-well plates (Becton, Dickinson and Company, Franklin Lakes, NJ) with 5×10^5 spleen cells from B6 and B6/*lpr* mice on a 0.4- μ m pore cell culture insert (Becton, Dickinson and Company). Co-culture was performed with RPMI-1640 (Wako Pure Chemical Industries) including 10% FBS for 48 h. The spleen cells were analyzed by flow cytometry. In addition, 5×10^4 B16F10/mGM cells were co-cultured with 1×10^4 spleen cells from B6 and B6/*lpr* mice for 24 h, and then VEGF mRNA expression of B16F10/mGM cells was detected by real

time-RT-PCR.

Western Blot Analysis

Tissues were homogenized and lysed in lysis buffer (50 mM Tris-HCl pH7.5, 250 mM NaCl, 0.1% Triton X-100, and 1mM EDTA) supplemented with protease inhibitor cocktail (Sigma-Aldrich Co. LLC., St. Louis, MO, USA). Protein concentration in Bio-Rad protein assay dye reagent concentrate (Bio-Rad Laboratories, Inc.) was determined by measuring the absorption at 595 nm on a microplate reader (Bio-Rad Laboratories, Inc.) A total of 20 µg of each sample per well was subjected to 10% sodium dodecyl sulfate–polyacrylamide gel electrophoresis gel and blotted onto nitrocellulose membranes (GE Healthcare, Buckinghamshire, UK). After blocking with 3% nonfat dry milk, the membranes were incubated with anti-HIF-1 α mAb overnight at 4°C, followed by washing and the addition of a HRP-conjugated secondary antibody for 1 h. Protein bands were visualized using an Immobilon Western Chemiluminescent HRP Substrate (Merck KGaA, Darmstadt, Germany). Densitometric analysis was performed to determine the ratio of HIF-1 α relative to β -actin.

Statistical Analysis

The results are presented as means \pm standard deviations (SDs). Comparisons of the results obtained for two groups were performed using an unpaired, two-tailed Student's *t*-test. *P* < 0.05 was considered significant.

RESULTS

Transplantation of Melanoma into B6/*lpr* Mice

We used B16F10 melanoma cells that are more metastatic and aggressively proliferative than the parental cell line B16F1.²¹ B16F10 melanoma cells were injected subcutaneously into C57BL/6 (B6) and B6/*lpr* mice. The recipient mice were analyzed 3 weeks after the injection. The findings of the CT analysis indicated that there was no difference in the size of the transplanted tumors between B6 and B6/*lpr* recipients (Figure 1a). In addition, there was no significant difference in the weight of tumor masses in the B6 and B6/*lpr* recipient mice (Figure 1b). Infiltrating immune cells, including CD3⁺ T cells, CD19⁺ B cells, NK1.1⁺CD3⁻ NK cells, F4/80⁺CD11b⁺ macrophages, F4/80⁺CD11b⁺CD11c⁺CD206⁻ M1 macrophages, and F4/80⁺CD11b⁺CD11c⁻CD206⁺ M2 macrophages among CD45.2⁺ cells in the tumor tissue were analyzed by flow cytometry (Supplementary Figure S1a). There were no significant differences in the cell number of T, B, NK cells, F4/80⁺CD11b⁺ macrophages, and M2 macrophages between B6 and B6/*lpr* recipient mice (Supplementary Figure S1b) whereas the number of M1 macrophages in B6/*lpr* recipient mice was significantly decreased compared with that of B6 control recipients (Supplementary Figure S1b). Moreover, no significant difference was found in the Ki67⁺ proliferating tumor cells in both types of recipient mice (Supplementary Figure S1c and S1d). Although these results indicate that the autoimmune had no effect on the growth of aggressively proliferative B16F10 melanoma cells, there might be any deficiency of differentiation or migration of M1 phenotype tumor-associated macrophages (TAMs).

Therefore, we next focused on TAMs. In order to activate M1 macrophages *in vivo*, granulocyte macrophage-colony stimulating factor (GM-CSF)-overexpressing B16F10 (B16F10/mGM) cells were transplanted subcutaneously into B6 and B6/*lpr* mice. It has been reported that the syngeneic transplantation of B16F10/mGM cells leads to the suppression of tumor growth and lung metastasis.²² Interestingly, the volume and weight of the tumors in B6/*lpr* recipient mice were significantly higher compared with those in the control recipients (Figure 1c and 1d). In addition, the survival rate of the B6/*lpr* recipient mice decreased to 60% at 3 weeks after tumor injection, whereas all of the B6 recipient mice were alive (Figure 1e).

Histopathological analysis showed that the focus of necrosis in transplanted B16F10/mGM cells was markedly observed in B6/*lpr* recipients (Figure 2a, upper panel). Moreover increased abnormal mitosis was also observed in B6/*lpr* recipients (Figure 2a, lower panel). The number of tumor cells that exhibited abnormal mitosis in B6/*lpr* recipient mice was significantly higher compared with that in B6 mice (Figure 2b). In addition, the number of Ki-67⁺ proliferating tumor cells in B6/*lpr* mice was significantly higher than that in B6 mice (Figure 2c and 2d). These findings suggest that tumor development may be enhanced in an autoimmunity model through the change of tumor environment.

Macrophages in Transplanted Tumor

The immune cell populations in transplanted B16F10/mGM tumor tissues were analyzed by flow cytometry (Supplementary Figure S2a). There was no difference in

the proportion of CD11b⁺F4/80⁺ TAMs and CD11b⁺F4/80⁺CD11c⁺CD206⁻ M1 (anti-tumor) TAMs in between B6 and B6/*lpr* mice (Figure 3a–d). By contrast, the proportion of CD11b⁺F4/80⁺CD11c⁻CD206⁺ M2 TAMs in B6/*lpr* recipient mice was significantly higher compared with that in control recipient mice (Figure 3b and 3e). The number of CD11b⁺F4/80⁺ TAMs in B6/*lpr* recipient mice was significantly lower compared with that in control recipient mice (Figure 3f). In addition, the number of CD11b⁺F4/80⁺CD11c⁺CD206⁻ M1 (anti-tumor) TAMs in B6/*lpr* recipient mice was significantly lower compared with that in B6 control recipient mice (Figure 3g). Although there was no difference in the number of CD11b⁺F4/80⁺CD11c⁻CD206⁺ M2 TAMs in B6 and B6/*lpr* mice (Figure 3h), the total number of M2 TAMs in whole tumor mass, not the cell number/g, in B6/*lpr* recipients was significantly higher compared with that in B6 recipients (Supplementary Figure S2b). In addition, the M1/M2 ratio of TAMs in B6/*lpr* recipient mice was reduced significantly compared with that in B6 mice (Figure 3i). However, there were no differences in the numbers of CD3⁺ T cells, CD19⁺ B cells, and NK1.1⁺CD3⁻ NK cells in the tumor tissues of B6 and B6/*lpr* recipient mice (Supplementary Figure S2c). Also, there was no difference in the number of CD11b⁺Gr-1⁺ myeloid-derived suppressor cells in the tumor tissues of B6 and B6/*lpr* recipient mice (Supplementary Figure S2d). Thus, it is possible that tumor immunity in this model may be dependent on the balanced accumulation of M1 and M2 TAMs.

M1 and M2 Macrophage-Related Gene Expression Levels

The mRNA expression levels of M1-related or M2-related cytokines were analyzed by

real-time RT-PCR (Figure 4). The mRNA expression levels of M1-related cytokines, such as IFN- γ , TNF- α , and MCP-1 were significantly lower in transplanted tumors in B6/*lpr* recipients compared with those in B6 recipients (Figure 4a). The mRNA expression levels of M2-related genes, such as Arg-1 and Fizz-1, were significantly lower in transplanted tumors in B6/*lpr* recipients compared with those in B6 recipients (Figure 4b). The mRNA expression level of TGF- β and Ym1 of the transplanted tumor tissues of B6/*lpr* recipients was significantly enhanced compared with that in B6 recipients (Figure 4b). These findings suggest that B6/*lpr* recipients exhibited deficiencies in the accumulation and function of M1 TAMs, and thus there might have been a partial dysfunction of M2 TAMs in B6/*lpr* recipients. By contrast, we analyzed mRNA expression of IFN- γ and TNF- α of spleen in B6 and B6/*lpr* mice transplanted with tumor (Supplementary Figure S3). IFN- γ mRNA expression of spleen in B6/*lpr* was significantly increased compared with that in B6 mice (Supplementary Figure S3). In addition, it was reported that IFN- γ level of sera in B6/*lpr* mice was significantly higher than that in control mice.²³ Therefore, the environment in tumor tissue may be different from the peripheral condition in this model.

To understand the differentiation of peripheral macrophages into M1 macrophages in B6/*lpr* mice in the presence of GM-CSF, the spleen cells from B6 and B6/*lpr* mice were co-cultured with B16F10 or B16F10/mGM cells using a chamber system. After co-culture with B16F10/mGM cells, the F4/80⁺CD11b⁺ macrophages among spleen cells from B6 mice increased significantly whereas there was no change in those from B6/*lpr* mice (Figure 4c, Supplementary Figure S4a). The proportion of CD11c⁺CD206⁻

M1 macrophages among F4/80⁺CD11b⁺ cells in B6/*lpr* mice co-cultured with B16F10/mGM cells was reduced significantly compared with that in B6 mice (Figure 4d, Supplementary Figure S4b). By contrast, the CD11c⁻CD206⁺ M2 macrophages in B6/*lpr* mice co-cultured with B16F10 cells increased significantly compared with that in B6 mice (Figure 4e). There was no difference in the M2 macrophages co-cultured with B16F10/mGM cells in B6 and B6/*lpr* mice (Figure 4e). Furthermore, the M1/M2 ratio of spleen cells in B6/*lpr* mice co-cultured with B16F10/mGM cells was significantly lower than that in B6 mice (Figure 4f). These findings suggest that an imbalance in differentiation into M1/M2 macrophages is associated with *in vivo* tumor growth in B6/*lpr* recipients.

In addition, we analyzed the mRNA expression of GM-CSF receptor *Csf2ra* of the transplanted tumor tissues in B6 and B6/*lpr* recipients. There was no difference in the mRNA expression level of *Csf2ra* in the tumor tissues between B6 and B6/*lpr* recipients (Supplementary Figure S5a). Moreover, spleen cells from B6 and B6/*lpr* mice were cultured in the presence of GM-CSF for 48 h to promote differentiation into M1 macrophage. Although the proportion of F4/80⁺CD11b⁺ cells in response to GM-CSF (10 and 50 ng/ml) in B6/*lpr* mice was significantly lower than that in B6 mice (Supplementary Figure S5b), there was no difference in the proportion of CD11c⁺CD206⁻F4/80⁺CD11b⁺ M1 macrophage and a M1/M2 ratio between B6 and B6/*lpr* mice (Supplementary Figure S5c, d, e). These findings suggest that the impaired function and accumulation of M1 TAMs in B6/*lpr* mice is not only by GM-CSF but also by the other factor in the environment of autoimmunity.

Tumor Angiogenesis in B6/*lpr* Recipient Mice

Regarding to enhanced tumor growth in B6/*lpr* recipients, several effects by TAMs were considered, which are a dysfunction of cytotoxic activity by TAMs, an enhanced effect on proliferation of tumor cells by TAMs, and promoted angiogenesis by TAMs. Thus, we investigated the *in vitro* cytotoxicity of spleen cells against B16F10/mGM cells. We found that there was no difference in the tumor cytotoxicity of spleen cells in both B6 and B6/*lpr* mice (Supplementary Figure S6a), thereby indicating that there was no effect of the autoimmune response in B6/*lpr* mice on the direct cytotoxic activity against tumor cells. In addition, there was no effect of spleen cells including macrophages on the proliferation of B16F10/mGM cells by *in vitro* co-culture assay (Supplementary Figure S6b). Therefore, we focused on the effect of TAMs on angiogenesis in B6/*lpr* mice. To elucidate tumor angiogenesis, immunofluorescence analysis was performed to detect CD31⁺ endothelial cells. There were increases in CD31⁺ endothelial cells in B6/*lpr* recipient mice compared with the control recipient mice (Figure 5a). The number of vessels in the tumor tissue of B6/*lpr* recipient mice was significantly higher compared with that in the control recipient mice (Figure 5b). In addition, VEGF, one of key factors for angiogenesis, was quantified by ELISA in the tumor tissues. A significantly higher level of VEGF protein was detected in the tumor tissue from B6/*lpr* recipient mice compared with that from the control recipient mice (Figure 5c). Moreover, the VEGF mRNA expression level in the tumor tissue from B6/*lpr* recipient mice was significantly higher than that from the control recipient mice (Figure 5d).

There was a correlation between the VEGF mRNA expression level and tumor weight in both B6 and B6/*lpr* recipient mice (Figure 5e), but the correlation between VEGF mRNA expression and tumor weight was considerably stronger in B6/*lpr* recipient mice than that in B6 recipient mice (Figure 5e). Furthermore, we performed additional experiments with transplantation of less aggressive tumor cells, B16F1 cells, and mouse lung cancer cell line, 3LL cells. Significantly increased weight of transplanted B16F1 and 3LL tumor mass of B6/*lpr* recipient mice were observed compared with that of control recipient mice (Supplementary Figure S7a, d). In addition, the number of CD31⁺ vessels in the 3LL and B16F1 tumor tissue of B6/*lpr* recipient mice was significantly higher compared with that in the control recipient mice (Supplementary Figure S7b, c, e). By contrast, there was no difference in the number of vessels in transplanted B16F10 at 3 weeks after tumor injection between B6 and B6/*lpr* recipients (Supplementary Figure S8). These results suggest that enhanced angiogenesis contributes to accelerated tumor growth in B6/*lpr* recipient mice.

Molecular Mechanism of Increased VEGF Expression in B6/*lpr* Recipient Mice

To examine whether tumor cells can produce VEGF by the interaction with immune cells including macrophages, B16F10/mGM cells were co-cultured with spleen cells of B6 and B6/*lpr* mice, and then VEGF mRNA expression of the tumor cells was measured by real time-RT-PCR. VEGF mRNA expression of B16F10/mGM cells co-cultured with spleen cells of B6/*lpr* mice was significantly enhanced compared with that of B6 mice (Figure 6a). In addition, when determining the distribution of VEGF

expression by immunofluorescence analysis, it was found that the expression of tumor tissue in the control recipient mice was localized to the tumor stromal tissue (Figure 6b). By contrast, VEGF in the tumor tissue of B6/*lpr* recipient mice was expressed in both tumor cells and stromal tissue (Figure 6b). On the other hand, we analyzed VEGF mRNA expression of B16F10/mGM and B16F10 cells. VEGF mRNA expression of B16F10/mGM cells was significantly lower than that of B16F10 cells (Supplementary Figure S9), suggesting that GM-CSF may regulate the expression of VEGF from tumor cells. As shown in Figure 2a, considerable tumor necrosis was observed in the tumor tissue from B6/*lpr* recipient mice. Therefore, we considered that hypoxia as well as accelerated tumor growth might be induced in the tumor tissue of B6/*lpr* recipient mice. To detect hypoxia in tumor cells, pimonidazol was injected intravenously as a hypoxia marker molecule into mice with transplanted tumors. At 30 min after of pimonidazol injection, the tumor tissues were fixed and hypoxic cells were detected by immunofluorescence analysis using anti-pimonidazol polyclonal antibody. Focal hypoxic cells were observed in the tumor tissues of B6 recipient mice (Figure 6c), whereas hypoxic cells were widespread and observed diffusely in the tumor tissues from B6/*lpr* recipient mice (Figure 6c). Hypoxic area (%) in the tumor tissues from B6/*lpr* recipient mice was significantly larger than that from B6 recipient mice (Figure 6d). In addition, it is well known that hypoxia-inducible factor-1 α (HIF-1 α) activates the transcription of VEGF in tumor cells²⁴ and higher expression level of HIF-1 α was found in the tumor tissues of B6/*lpr* recipient mice compared with the control recipient mice (Figure 6e). The increased expression level of HIF-1 α in the transplanted tumor tissues

of B6/*lpr* recipients was also confirmed by Western blotting (Figure 6f and 6g). These results suggest that the enhancement of angiogenesis via the upregulation of VEGF by HIF-1 α help to promote tumor growth in an animal model of autoimmunity.

Enhanced angiogenesis in B16F1 and 3LL tumor tissues in B6/*lpr* recipients

To further understand the mechanism of enhanced angiogenesis in B6/*lpr* recipients, when we analyzed the number of vessels in the early stage (10 days after injection of B16F10/mGM cells) in which there was no difference in tumor size between B6 and B6/*lpr* mice (Figure 7a), the number of vessels, hypoxic area, and HIF-1 α expression in the tumor tissue of B6/*lpr* recipient mice were significantly higher compared with those in the control recipient mice (Figure 7b, c, d, Supplementary Figure S10a, b, c). In addition, VEGF expression in the tumor tissue of B6/*lpr* recipient mice was significantly higher compared with that in the control recipient mice (Figure 7e, Supplementary Figure S10d). Therefore, enhanced angiogenesis in B6/*lpr* recipients was not caused by different size of transplanted tumors.

Discussion

Previously, it was reported that there is a clear increased risk of malignant lymphoma and cancers of the vulva, lung, and thyroid gland in patients with autoimmune diseases.¹⁷⁻²⁰ In addition, a meta-analysis demonstrated an increased risk of malignant lymphoma and lung cancer in patients with RA.²⁵ There are several possible explanations for the link between lymphoma and autoimmune diseases.^{26,27} It is known

that translocations involving the juxtaposition of an oncogene adjacent a gene that is important for immune cell function may be associated with the onset of lymphoma.^{28,29} The alterations caused by translocation are proportional to the rate of lymphocyte proliferation, which may explain the increased risk of lymphoma in autoimmune diseases. It has also been reported that mucosa-associated lymphoid tissue lymphoma is the most common lymphoma in primary Sjögren's syndrome.³⁰ However, the precise mechanism that underlies this association remains unclear, and thus it is difficult to understand the relationship between tumors other than lymphoma and autoimmunity. In this study, we analyzed TAMs in *B6/lpr* mice in a transplantation experiment with GM-CSF-overexpressing melanoma cell line. We also investigated the molecular mechanism of tumor growth in *B6/lpr* mice. A lot of reports demonstrate that immunological tolerance contributes controlling tumor immunity.^{31,32} However, in some reports, both merit and demerit effects on anti-tumor immunity were described.^{32,33} Our results demonstrate that the environment in autoimmunity contributes to the growth of transplanted tumor through disorder of M1 TAM accumulation or enhanced angiogenesis. On the other hand, as the effect of autoimmune response on anti-tumor immunity in spontaneously occurring models is unclear, further study would be helpful for understanding the complicated tumor immunity system.

Macrophages play a key role in the link between inflammation and carcinogenesis^{4,34,35}, and many studies have demonstrated that TAMs promote tumor progression.^{8,36} For example, the overexpression of CCL2 by murine fibroblast cells leads to increased TAM infiltration, which promotes tumor growth in a mouse model.³⁷

In addition, macrophages play a crucial role in regulating tumor growth, survival, metastasis of tumor cells, angiogenesis, and immunosuppression.^{34,35} Several studies have found that TAMs exhibit an IL-12 low/IL-10 high phenotype with upregulated VEGF, EGF, COX2, and MMPs, which promote tumor growth.³⁸⁻⁴⁰ In the present study, GM-CSF-overexpressing melanoma cells were transplanted into B6/*lpr* mice to promote the accumulation of monocytes or macrophages in the tumor tissues. The lower number of M1 TAMs in B6/*lpr* mice demonstrated the insufficient anti-tumor function of TAMs whereas there were no differences in the numbers of infiltrating T, B, and NK cells in the tumor tissues of B6/*lpr* mice. These findings suggest that the tumor immune system is impaired in the condition of autoimmunity. It is possible that the insufficient accumulation of TAMs in B6/*lpr* mice may disrupt the network of tumor immunity as well as decreasing the control of tumor growth. However, the precise cellular or molecular mechanisms that underlie the disruption of tumor immunity remain unclear.

GM-CSF is one of the key factors involved in the activation of macrophages or dendritic cells.²² In particular, GM-CSF derived from tumor cells stimulates the secretion of macrophage metalloelastase and the production of angiostatin by tumor-infiltrating macrophages, which are associated with tumor growth and metastasis.⁴¹ In this study, there was no significant difference in B6 and B6/*lpr* recipient mice transplanted with B16F10 cells, although the tumor weight was significantly higher in B6/*lpr* mice transplanted with B16F10/mGM cells. As described in previous studies²², tumor growth of B16F10/mGM cells was significantly lower in both B6 and B6/*lpr* mice compared with that of B16F10 in this study. The findings suggest that

GM-CSF produced from B16F10/mGM cells attract and activate macrophages in the tumor environment. Moreover, we confirmed the enhanced growth of less progressive B16F1 and 3LL cells in B6/*lpr* recipients similar to B16F10/mGM cells. As shown in Figure 1, the tumor weight of B16F10 cells in both B6 and B6/*lpr* recipients was roughly twice as large as that of B16F10/mGM cells. Anti-tumor effect of GM-CSF in B16F10/mGM cells has been reported.²² Therefore, the discrepancy in the cell number of M2 TAMs between transplanted B16F10 and B16F10/mGM cells might be caused by the difference of tumor growth. Moreover, it was reported that target deletion of Fas in CD11b⁺ myeloid cells could greatly enhance the number of activated proinflammatory macrophages.⁴² However, it is still unclear why the macrophages from B6/*lpr* are resistant to attraction and activation by GM-CSF in the tumor environment.

It is well known that autoimmunity is a multifactorial disease.⁹⁻¹² Thus, various immune cells contribute to the onset or development of autoimmune disease. In patients with SLE, there is an increase in the spontaneous appearance of apoptotic cells within lymph nodes and blood, thereby suggesting that an increase in apoptotic cells reflects an impairment in the capacity of phagocytes, including macrophages or dendritic cells, to engulf dead cells.^{14,43,44} Mice that lack milk fat globule-epidermal growth factor 8 gene accumulate apoptotic lymphocytes within lymph nodes and they develop an SLE-like disease, which involves autoantibody formation, splenomegaly, and glomerulonephritis.^{45,46} Macrophages are prominent within the inflamed kidney and they are key mediators of lupus nephritis in *lpr* mice.⁴⁷⁻⁴⁹ In addition, M1 macrophages contribute to the onset of SLE-like lesions in the kidneys of *lpr* mice.⁵⁰ Our result

demonstrated that the cell number of M1 TAMs was reduced in B6/*lpr* mice, whereas there was no difference in the cell number of M2 TAMs in between B6 and B6/*lpr* mice. The environment in which M1 TAMs are reduced and M2 TAMs are increased tends to be an immunosuppressive condition. Our result indicated that increased mRNA expression of cytokines produced from M1 TAMs, decreased M2-related gene expression, and a reduction of M1/M2 ratio in the transplanted tumor tissues of B6/*lpr* recipients may result in the induction of more immunosuppressive condition in the model. This suggests that the polarization of M1/M2 macrophage in the tumor tissues of B6/*lpr* mice differ from that in autoimmune lesions, thereby implying that both autoimmunity and the tumor microenvironment influence the polarization of M1/M2 macrophages.

VEGF production by tumor and stromal cells has various functions in the tumor microenvironment.⁵¹ In particular, VEGF functions as a primary stimulus during angiogenesis, where it induces the proliferation and migration of endothelial cells, as well as remodeling of the extracellular matrix, thereby allowing the formation of new blood vessels and increased vascular permeability. By contrast, VEGF production by tumor cells functions in an autocrine manner to promote dedifferentiation and an epithelial-mesenchymal transition phenotype that enhances tumor invasion and survival.⁴⁸ VEGF production is related to the response to hypoxia via HIF-1 α .^{23,52,53} Our results showed that both tumor and stromal cells expressed VEGF in the tumor tissues of B6/*lpr* mice, whereas VEGF was expressed in the stromal cells in the tumor tissues of B6 mice. In addition, increased hypoxia and upregulated HIF-1 α expression were

observed in the tumor tissues of *B6/lpr* mice. It is possible that the initial proliferation of tumor cells due to the impaired accumulation of M1 macrophages may be promoted in *B6/lpr* mice, whereas VEGF expression in tumor cells may be upregulated via hypoxia by increased HIF-1 α expression due to excessive tumor growth. In this model, M2 TMAs may play an important role in the enhanced angiogenesis. However, its precise mechanism in the unique environment in autoimmunity is still unclear.

Regarding Fas deficiency in *B6/lpr*, FasL is expressed on immune cells in *B6/lpr* mice. There seems to be no effect of the FasL expression in *B6/lpr* recipients on growth of transplanted tumor as it was reported that no effect of injection of anti-FasL blocking antibody was observed on tumor growth in some models.⁵⁴ Therefore, the enhancement of tumor growth in *B6/lpr* recipient may be caused by autoimmune inflammation, rather than by the deficiency of Fas.

In summary, M1 macrophage dysfunction during the response to GM-CSF and enhanced angiogenesis via hypoxia and VEGF upregulation may contribute to increased tumor growth in *B6/lpr* mice (Supplementary Figure S11). Our results suggest that autoimmunity may disrupt tumor immunity to promote tumor growth.

DISCLOSURE/CONFLICT OF INTEREST

The authors declare no conflict of interest.

Acknowledgments

This study was supported by JSPS Grants-in-Aid for Scientific Research (15K15676, 15K15740), Grant-in-Aid for JSPS Fellows, Uehara Memorial Foundation, and Takeda Science Foundation.

References

1. Folkman J. Tumor angiogenesis: therapeutic implications. *N Engl J Med* 1971;285:1182-6.
2. Motz GT, Coukos G. Deciphering and reversing tumor immune suppression. *Immunity* 2013;39:61-73.
3. Darcy PK, Neeson P, Yong CS, Kershaw MH. Manipulating immune cells for adoptive immunotherapy of cancer. *Curr Opin Immunol* 2014;27:46-52.
4. Noy R, Pollard JW. Tumor-associated macrophages: from mechanisms to therapy. *Immunity* 2014;41:49-61.
5. Biswas SK, Chittezhath M, Shalova IN, *et al.* Macrophage polarization and plasticity in health and disease. *Immunol Res* 2012;53:11-24.
6. Mantovani A, Biswas SK, Galdiero MR, *et al.* Macrophage plasticity and polarization in tissue repair and remodelling. *J Pathol* 2013;229:176-85.
7. Gordon S, Martinez FO. Alternative activation of macrophages: mechanism and functions. *Immunity* 2010;32:593-604.
8. Mantovani A, Sozzani S, Locati M, *et al.* Macrophage polarization: tumor-associated macrophages as a paradigm for polarized M2 mononuclear phagocytes. *Trends Immunol* 2002;23:549-55.
9. Morel L. Genetics of SLE: evidence from mouse models. *Nat Rev Rheumatol* 2010;6:348-57.
10. Kobezda T, Ghassemi-Nejad S, Mikecz K, *et al.* Of mice and men: how animal models advance our understanding of T-cell function in RA. *Nat Rev Rheumatol* 2014;10:160-70.
11. Klareskog L, Padyukov L, Lorentzen J, *et al.* Mechanisms of disease: Genetic susceptibility and environmental triggers in the development of rheumatoid arthritis.

- Nat Clin Pract Rheumatol 2006;2:425-33.
12. Scher JU, Abramson SB. The microbiome and rheumatoid arthritis. *Nat Rev Rheumatol* 2011;7:569-78.
 13. Ayoub S, Hickey MJ, Morand EF. Mechanisms of disease: macrophage migration inhibitory factor in SLE, RA and atherosclerosis. *Nat Clin Pract Rheumatol* 2008;4:98-105.
 14. Poon IK, Lucas CD, Rossi AG, *et al.* Apoptotic cell clearance: basic biology and therapeutic potential. *Nat Rev Immunol* 2014;14:166-80.
 15. Moreno M, Bannerman P, Ma J, *et al.* Conditional ablation of astroglial CCL2 suppresses CNS accumulation of M1 macrophages and preserves axons in mice with MOG peptide EAE. *J Neurosci* 2014;34:8175-85.
 16. Iwasa A, Arakaki R, Honma N, *et al.* Aromatase controls Sjogren syndrome-like lesions through monocyte chemotactic protein-1 in target organ and adipose tissue-associated macrophages. *Am J Pathol* 2015;185:151-61.
 17. Azizi G, Malchoff CD. Autoimmune thyroid disease: a risk factor for thyroid cancer. *Endocr Pract* 2011;17:201-9.
 18. Bernatsky S, Ramsey-Goldman R, Labrecque J, *et al.* Cancer risk in systemic lupus: an updated international multi-centre cohort study. *J Autoimmun* 2013;42:130-5.
 19. Bin J, Bernatsky S, Gordon C, *et al.* Lung cancer in systemic lupus erythematosus. *Lung cancer* 2007;56:303-6.
 20. Zintzaras E, Voulgarelis M, Moutsopoulos HM. The risk of lymphoma development in autoimmune diseases: a meta-analysis. *Arch Intern Med* 2005;165:2337-44 .
 21. Cillo C, Dick JE, Ling V, *et al.* Generation of drug-resistant variants in metastatic B16 mouse melanoma cell lines. *Cancer Res.* 1987;47(10):2604-8.
 22. Dong Z, Yoneda J, Kumar R, *et al.* Angiostatin-mediated suppression of cancer metastases by primary neoplasms engineered to produce granulocyte/macrophage colony-stimulating factor. *J Exp Med* 1998;188:755-63.
 23. Oura R, Arakaki R, Yamada A, *et al.* Induction of rapid T cell death and phagocytic activity by Fas-deficient *lpr* macrophages. *J Immunol* 2013;190:578-85.
 24. Collet G, El Hafny-Rahbi B, Nadim M, *et al.* Hypoxia-shaped vascular niche for cancer stem cells. *Contemp Oncol (Pozn)* 2015;19:A39-43.
 25. Smitten AL, Simon TA, Hochberg MC, *et al.* A meta-analysis of the incidence of malignancy in adult patients with rheumatoid arthritis. *Arthritis Res Ther*

- 2008;10:R45.
26. Bernatsky S, Ramsey-Goldman R, Rajan R, *et al.* Non-Hodgkin's lymphoma in systemic lupus erythematosus. *Ann Rheum Dis* 2005;64:1507-9.
 27. Dias C, Isenberg DA. Susceptibility of patients with rheumatic diseases to B-cell non-Hodgkin lymphoma. *Nat Rev Rheumatol* 2011;7:360-8.
 28. Sonoki T, Tatetsu H, Nagasaki A, *et al.* Molecular cloning of translocation breakpoint from der(8)t(3;8)(q27;q24) defines juxtaposition of downstream of C-MYC and upstream of BCL6. *Int J Hematol* 2007;86:196-8.
 29. Spehalski E, Kovalchuk AL, Collins JT, *et al.* Oncogenic Myc translocations are independent of chromosomal location and orientation of the immunoglobulin heavy chain locus. *Proc Natl Acad Sci U S A* 2012;109:13728-32.
 30. Boussios S, Pentheroudakis G, Somarakis G, *et al.* Cancer diagnosis in a cohort of patients with Sjogren's syndrome and rheumatoid arthritis: a single-center experience and review of the literature. *Anticancer Res* 2014;34:6669-76.
 31. Nishikawa H, Sakaguchi S. Regulatory T cells in tumor immunity. *Int J Cancer* 2010;127(4):759-67.
 32. Wei WZ1, Jacob JB, Zielinski JF, *et al.* Concurrent induction of antitumor immunity and autoimmune thyroiditis in CD4+ CD25+ regulatory T cell-depleted mice. *Cancer Res* 2005;65:8471-8.
 33. Melero I, Hervas-Stubbs S, Glennie M, *et al.* Immunostimulatory monoclonal antibodies for cancer therapy. *Nat Rev Cancer* 2007;7:95-106.
 34. Mantovani A, Allavena P, Sica A, *et al.* Cancer-related inflammation. *Nature* 2008;454: 36-44.
 35. Qian BZ, Pollard JW. Macrophage diversity enhances tumor progression and metastasis. *Cell* 2010;141:39-51.
 36. Lewis CE, Pollard JW. Distinct role of macrophages in different tumor microenvironments. *Cancer Res* 2006;66:605-12.
 37. Bottazzi B, Walter S, Govoni D, *et al.* Monocyte chemotactic cytokine gene transfer modulates macrophage infiltration, growth, and susceptibility to IL-2 therapy of a murine melanoma. *J Immunol* 1992;148:1280-5.
 38. Sica A, Saccani A, Bottazzi B, *et al.* Autocrine production of IL-10 mediates defective IL-12 production and NF-kappa B activation in tumor-associated macrophages. *J Immunol* 2000;164:762-7.

39. Biswas SK, Gangi L, Paul S, *et al.* A distinct and unique transcriptional program expressed by tumor-associated macrophages (defective NF-kappaB and enhanced IRF-3/STAT1 activation). *Blood* 2006;107:2112-22.
40. Hagemann T, Lawrence T, McNeish I, *et al.* "Re-educating" tumor-associated macrophages by targeting NF-kappaB. *J Exp Med* 2008;205:1261-8.
41. Dong Z, Kumar R, Yang X, *et al.* Macrophage-derived metalloelastase is responsible for the generation of angiostatin in Lewis lung carcinoma. *Cell* 1997;88:801-10.
42. Li J, Hsu HC, Mountz JD. Managing macrophages in rheumatoid arthritis by reform or removal. *Curr Rheumatol Rep* 2012;14:445-54.
43. Baumann I, Kolowos W, Voll RE, *et al.* Impaired uptake of apoptotic cells into tingible body macrophages in germinal centers of patients with systemic lupus erythematosus. *Arthritis Rheum* 2002;46:191-201.
44. Perniok A, Wedekind F, Herrmann M, *et al.* High levels of circulating early apoptic peripheral blood mononuclear cells in systemic lupus erythematosus. *Lupus* 1998;7:113-8.
45. Hanayama R, Tanaka M, Miyasaka K, *et al.* Autoimmune disease and impaired uptake of apoptotic cells in MFG-E8-deficient mice. *Science* 2004;304:1147-50.
46. Hu CY, Wu CS, Tsai HF, *et al.* Genetic polymorphism in milk fat globule-EGF factor 8 (MFG-E8) is associated with systemic lupus erythematosus in human. *Lupus* 2009;18:676-81.
47. Bloom RD, Florquin S, Singer GG, *et al.* Colony stimulating factor-1 in the induction of lupus nephritis. *Kidney Int* 1993;43:1000-9.
48. Kelley VE, Wing E. Loss of resistance to listeria infection in autoimmune MRL/lpr mice: protection by prostaglandin E1. *Clin Immunol Immunopathol* 1982;23:705-10.
49. Menke J, Rabacal WA, Byrne KT, *et al.* Circulating CSF-1 promotes monocyte and macrophage phenotypes that enhance lupus nephritis. *J Am Soc Nephrol* 2009;20:2581-92.
50. Iwata Y, Bostrom EA, Menke J, *et al.* Aberrant macrophages mediate defective kidney repair that triggers nephritis in lupus-susceptible mice. *J Immunol* 2012;188:4568-80.
51. Goel HL, Mercurio AM. VEGF targets the tumour cell. *Nat Rev Cancer*

2013;13:871-82.

52. Burke B, Tang N, Corke KP, *et al.* Expression of HIF-1alpha by human macrophages: implications for the use of macrophages in hypoxia-regulated cancer gene therapy. *J Pathol* 2002;196:204-12.
53. Zhong H, Chiles K, Feldser D, *et al.* Modulation of hypoxia-inducible factor 1alpha expression by the epidermal growth factor/phosphatidylinositol 3-kinase/PTEN/AKT/FRAP pathway in human prostate cancer cells: implications for tumor angiogenesis and therapeutics. *Cancer Res* 2000;60:1541-5.
54. Muraoka D, Kato T, Wang L, *et al.* Peptide Vaccine Induces Enhanced Tumor Growth Associated with Apoptosis Induction in CD8+ T Cells. *J Immunol* 2010;185(6):3768-76.

Figure Legends

Figure 1 Transplantation of B16F10 and B16F10/mGM melanoma into B6/*lpr* mice. **(a)** Analysis of tumor volume by computed tomography (CT) at 3 weeks after injection of B16F10 cells. Representative CT images from each group (n = 5) are shown. Scale bar = 1 cm. **(b)** Weights of transplanted tumor masses. **(c)** Analysis of tumor volume by CT at 3 weeks after injection of B16F10/mGM cells. Representative CT and macrograph images from each group (B6, n = 7; B6/*lpr*, n = 11) are shown. Scale bar = 1 cm. **(d)** Transplanted tumor volumes using CT image were analyzed (n=3). Transplanted tumor weights were measured (B6, n = 7; B6/*lpr*, n = 11). **(e)** Survival curves of B6 and B6/*lpr* recipient mice after injection of B16F10/mGM cells. **p* < 0.05. ***p* < 0.005.

Figure 2 Growth of B16F10/mGM cells in B6/*lpr* mice. **(a)** Histopathological analysis of transplanted tumor tissues of B6 and B6/*lpr* recipients. Representative images from

each group are shown. Scale bar = 100 μm or 50 μm . Arrow: mitotic cell. **(b)** Mitotic cells were counted per 1 mm^2 . **(c)** Ki-67⁺ proliferating cells were detected by immunofluorescence analysis. The nuclei were stained with DAPI. Scale bar = 100 μm . **(d)** Ki-67⁺ proliferating cells (%) in transplanted tumor tissues. The data represent the means \pm SD for each group. * $p < 0.05$.

Figure 3 Tumor-associated macrophages (TAMs) of transplanted B16F10/mGM cells in B6/*lpr* mice. **(a)** F4/80⁺CD11b⁺ TAMs in B6 and B6/*lpr* recipients were analyzed by flow cytometry. Each panel of the figure is representative of at least three independent experiments for each group (n = 3). **(b)** Proportion of F4/80⁺CD11b⁺CD11c⁺CD206⁻ M1 TAMs and F4/80⁺CD11b⁺CD11c⁻CD206⁺ M2 TAMs in B6 and B6/*lpr* recipients. **(c)** F4/80⁺CD11b⁺ TAMs (%) are shown as the means \pm SD for each group. **(d)** F4/80⁺CD11b⁺CD11c⁺CD206⁻ M1 TAMs (%) are shown as the means \pm SD for each group. **(e)** F4/80⁺CD11b⁺CD11c⁻CD206⁺ M2 TAMs (%) are shown as the means \pm SD for each group. **(f)** Number of F4/80⁺CD11b⁺ TAMs per tumor mass (g). **(g)** Number of F4/80⁺CD11b⁺CD11c⁺CD206⁻ M1 TAMs per tumor mass (g). **(h)** Number of F4/80⁺CD11b⁺CD11c⁻CD206⁺ M2 TAMs per tumor mass (g). **(i)** The M1/M2 ratios represent the means \pm SD for each group. * $p < 0.05$.

Figure 4 M1 and M2 macrophage-related gene expression and *in vitro* differentiation into M1 macrophages. **(a)** The mRNA expression levels of M1-related genes, including IFN- γ , TNF- α , IL-6, MCP-1, and IRF5 were detected by real-time RT-PCR in

transplanted tumor tissues from B6 and B6/*lpr* recipients. **(b)** The mRNA expression levels of IL-10, Arg-1, TGF- β , Ym1, and Fizz-1 in transplanted tumor tissues of B6 and B6/*lpr* recipients were detected by real-time RT-PCR. The data represent the mean of relative expression to F4/80 mRNA \pm SD of each group (n = 5). **(c)** Spleen cells of B6 and B6/*lpr* mice were co-cultured with B16F10 or B16F10/mGM cells for 48 h in inserted chamber wells. The proportion of F4/80⁺CD11b⁺ macrophages in cultured spleen cells was detected by flow cytometric analysis. **(d)** The proportion of CD11c⁺CD206⁻ M1 macrophages in F4/80⁺CD11b⁺ cells from cultured spleen cells was detected by flow cytometric analysis. **(e)** The proportion of CD11c⁻CD206⁺ M2 macrophages in F4/80⁺CD11b⁺ cells from cultured spleen cells was detected by flow cytometric analysis. **(f)** The M1/M2 ratio was determined. The data represent the means \pm SD for each group (n = 5) at least three independent experiments. **p* < 0.05.

Figure 5 Enhanced angiogenesis in the tumor tissues of B6/*lpr* recipients. **(a)** CD31⁺ cells from the tumor tissues in B6 and B6/*lpr* recipients were detected by immunofluorescence analysis. Representative photos from each group (n = 5) are shown. Scale bar = 100 μ m. **(b)** The number of CD31⁺ vessels was counted per 1 mm² tissue. **(c)** VEGF concentration in transplanted B16F10/mGM tumor tissues from B6 and B6/*lpr* recipients was measured by ELISA. The data represent the means \pm SD for each group (n = 5) at least three independent experiments. **p* < 0.05. **(d)** The mRNAs expression levels of VEGF in the transplanted tumor tissues from B6 and B6/*lpr* recipients. **(e)** Correlation between tumor weight and VEGF mRNA expression levels in

transplanted tumor tissue from B6 and B6/*lpr* recipients (n = 8). R^2 is the correlation coefficient; $R^2 > 0.7$ indicates a strong correlation.

Figure 6 VEGF expression and hypoxia via HIF-1 α in transplanted tumors. **(a)** B16F10/mGM cells were co-cultured with spleen cells of B6 and B6/*lpr* mice for 24 h. VEGF mRNA expression of B16F10/mGM cells was detected by real time-RT-PCR. Relative expressions to the expression of tumor cells co-cultured without spleen cells are shown as the means \pm SD for each group (n = 5). * $p < 0.05$. **(b)** VEGF expression in the transplanted tumor tissues from B6 and B6/*lpr* recipients, which was detected by immunofluorescence analysis. Representative photos from each group (n = 5) are shown. Scale bar = 100 μ m. **(c)** Hypoxia in transplanted tumor cells was detected by immunofluorescence analysis via intravenous injection of pimonidazol into recipient mice. Representative photos of each group (n = 5) are shown. Scale bar = 100 μ m. **(d)** Hypoxic area (%) in the tumor tissues was measured, and the data are shown as the means \pm SD (%) for each group (n = 5). * $p < 0.05$. **(e)** HIF-1 α expression in the transplanted tumor tissues from B6 and B6/*lpr* recipients, which was detected by immunofluorescence analysis. Representative images from each group (n = 5) are shown. Scale bar = 100 μ m. **(f)** HIF-1 α expression in the transplanted tumor tissues from B6 and B6/*lpr* recipients was detected by Western blotting. The data represent at least three independent experiments. **(g)** Expression of HIF-1 α relative to β -actin in the transplanted tumor tissues from B6 and B6/*lpr* mice according to Western blotting, which was measured based on the densitometric intensity. The data are shown as the

means \pm SD for each group (n = 5). * p < 0.05.

Figure 7 Angiogenesis of transplanted tumor at early stage in B6/*lpr* mice. **(a)** B16F10/mGM cells were injected subcutaneously into B6 or B6/*lpr* mice. At 10 days after injection, transplanted tumor weights were measured. The data are shown as the means \pm SD for each group (n = 4). **(b)** CD31⁺ cells from the tumor tissues in B6 and B6/*lpr* recipients were detected by immunofluorescence analysis. The number of CD31⁺ vessels was counted per 1 mm² tissue. The data are shown as the means \pm SD for each group (n = 4). * p < 0.05. **(c)** Hypoxia in transplanted tumor cells was detected by immunofluorescence analysis via intravenous injection of pimonidazol into recipient mice. Hypoxic area (%) in the tumor tissues was measured. **(d)** HIF-1 α ⁺ cells from the tumor tissues in B6 and B6/*lpr* recipients were detected by immunofluorescence analysis. HIF-1 α ⁺ cells (%) in transplanted tumor tissues were counted. The data are shown as the means \pm SD for each group (n = 4). * p < 0.05. **(e)** VEGF⁺ cells from the tumor tissues in B6 and B6/*lpr* recipients were detected by immunofluorescence analysis. VEGF⁺ cells (%) in transplanted tumor tissues were counted. The data are shown as the means \pm SD for each group (n = 4). * p < 0.05.

Figure 1

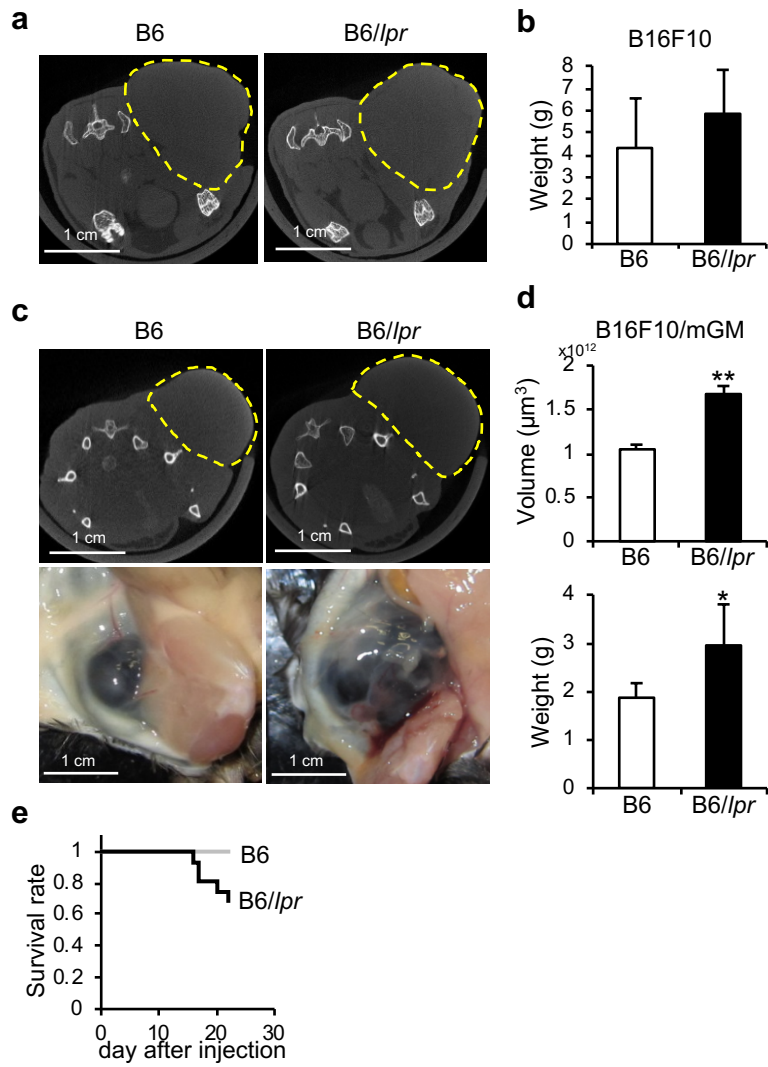


Figure 2

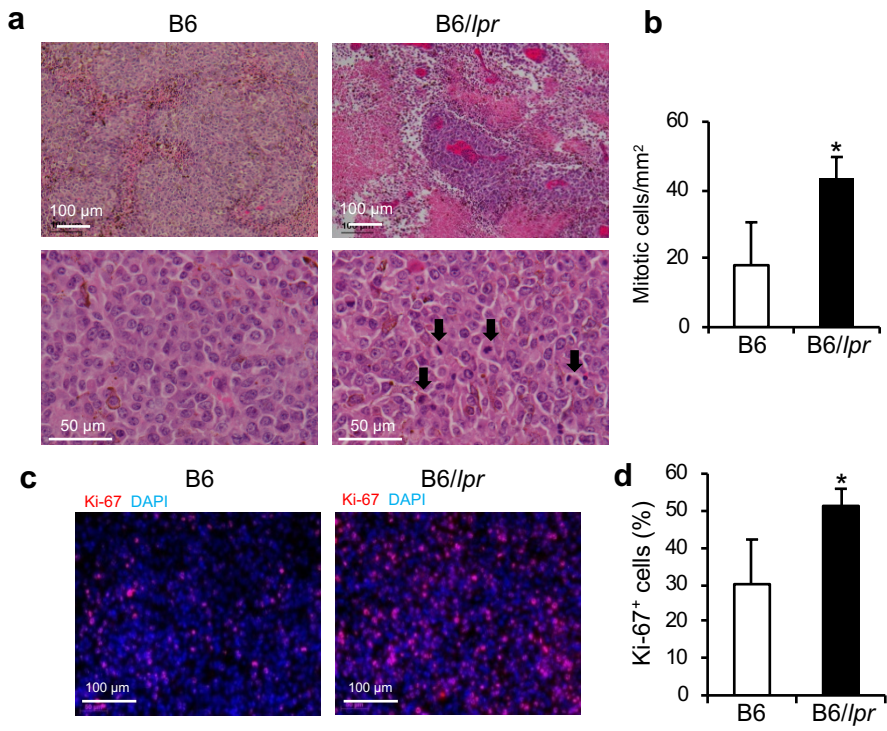


Figure 3

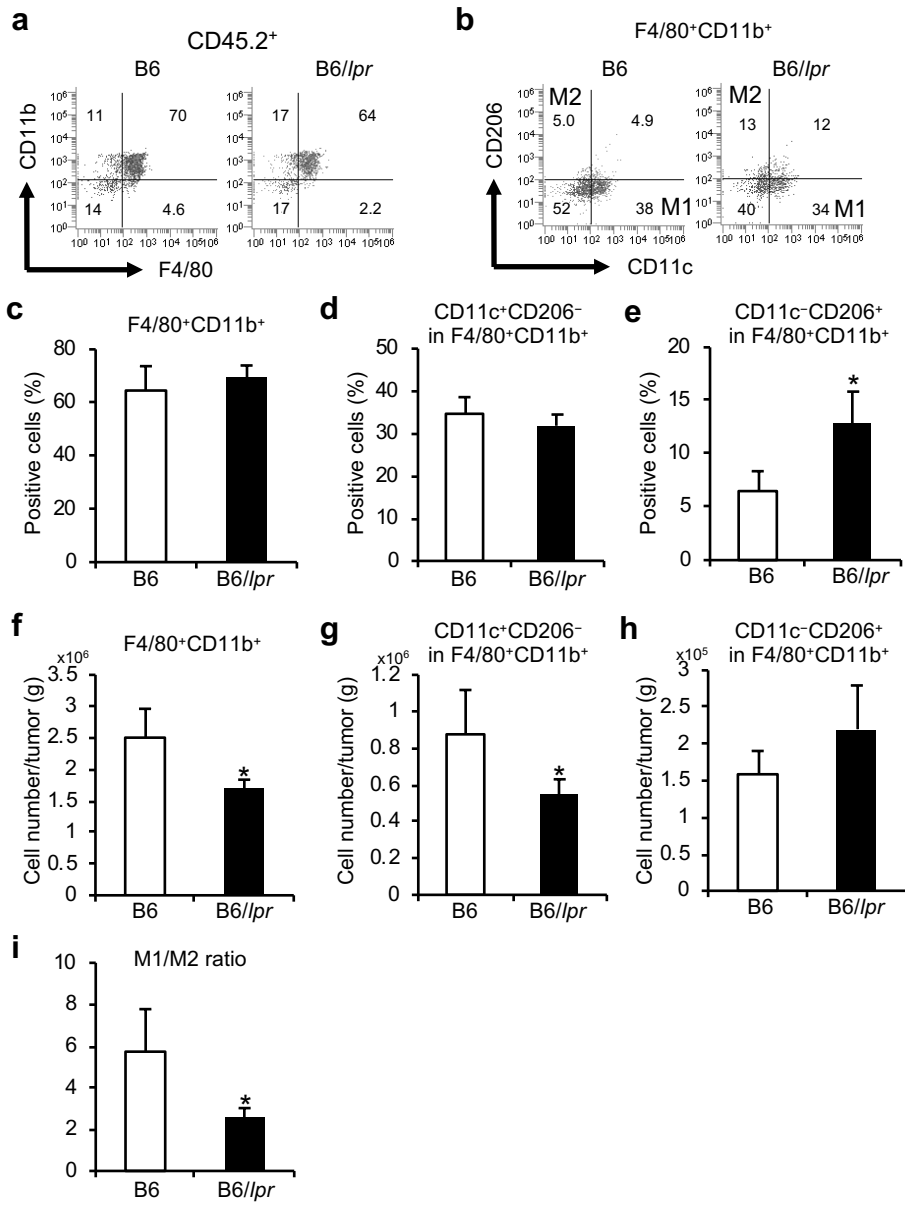


Figure 4

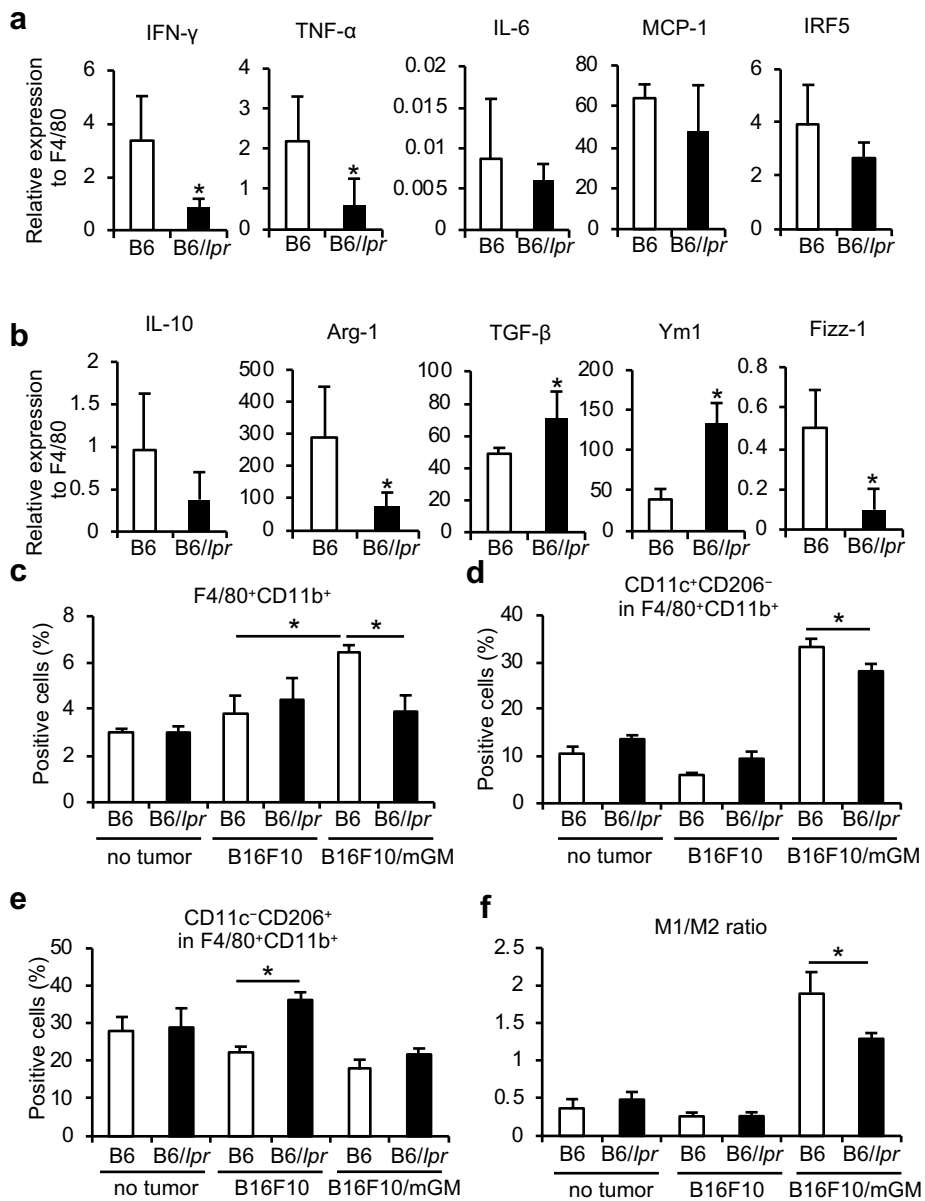


Figure 5

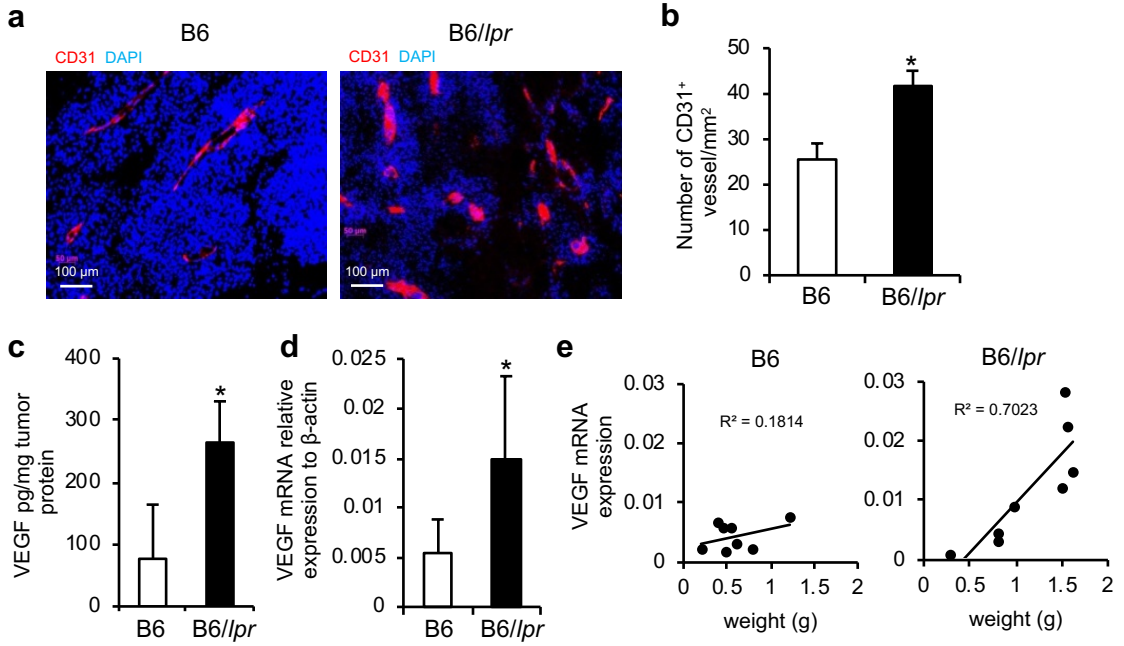


Figure 6

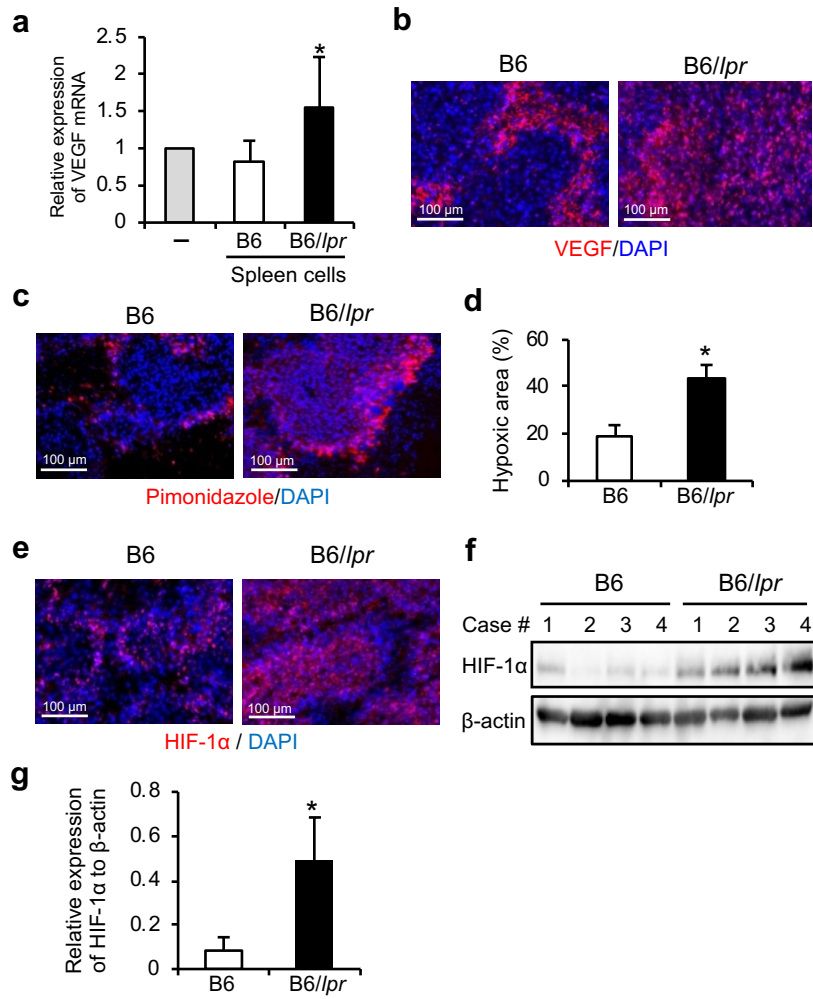
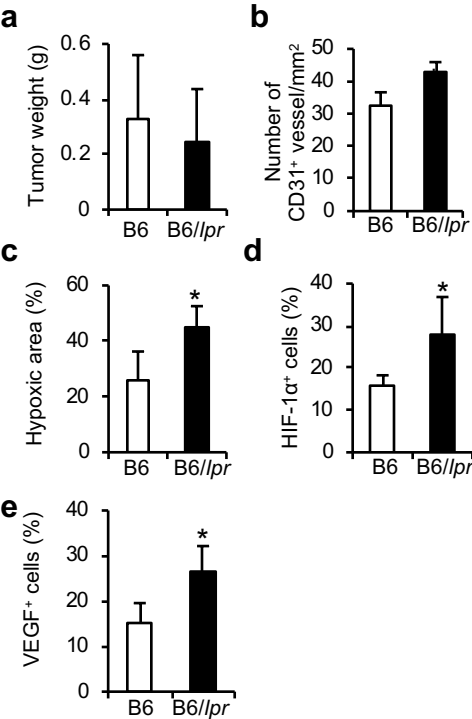


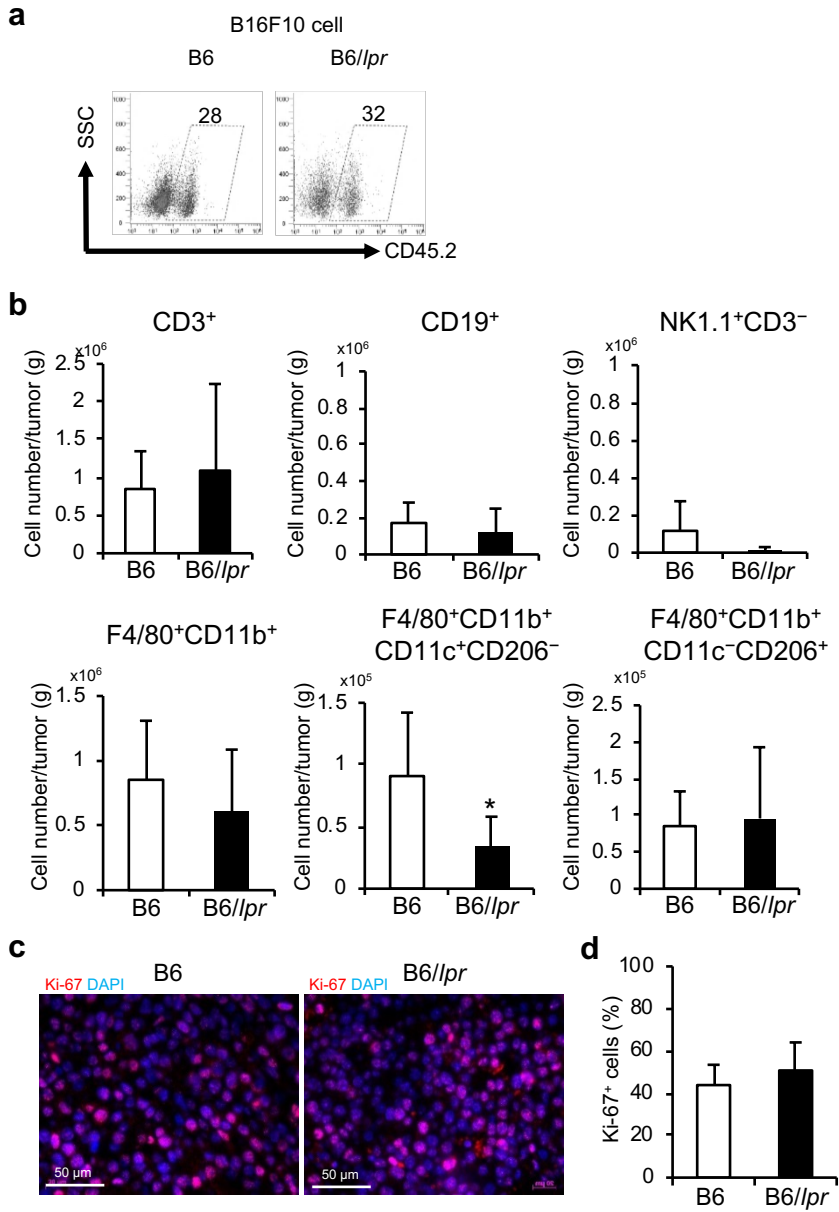
Figure 7



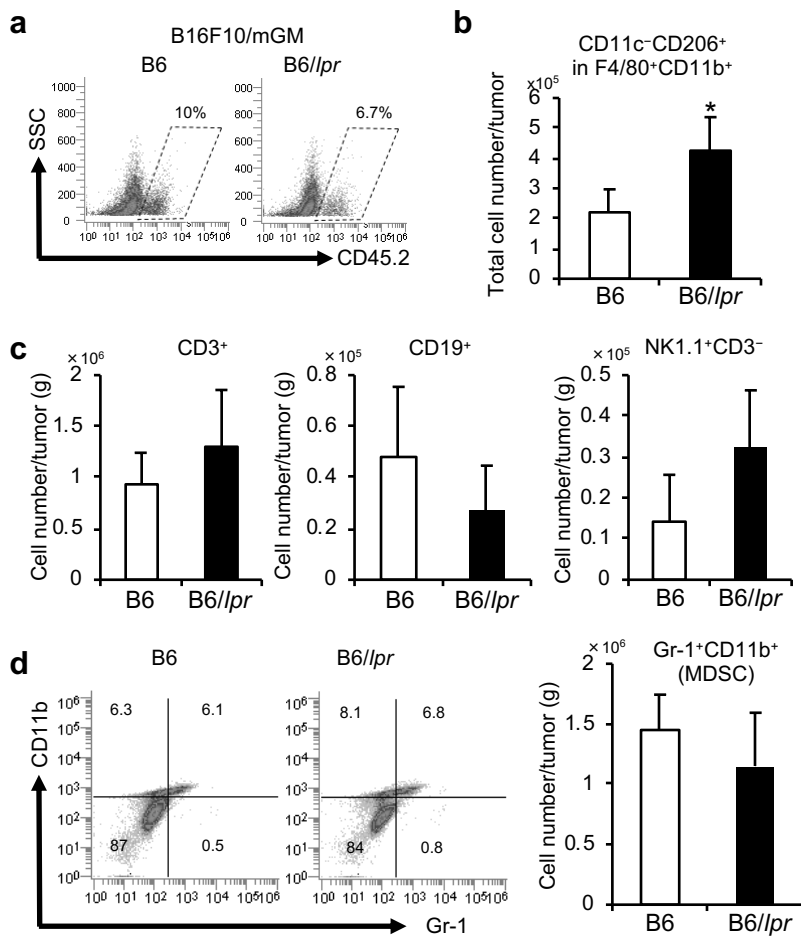
Supplementary Table S1

Gene	Forward	Reverse
IFN- γ	5'-AGCGGCTGACTGAACTCAGATTGTAG-3'	5'-GTCACAGTTTTTCAGCTGTATAGGG-3'
TNF- α	5'-ATGAGAAGTTCCCAAATGGC-3'	5'-CTCCACTTGGTGGTTTGCTA-3'
IL-6	5'-GCTACCAAACCTGGATATAATCAGGA-3'	5'-CCAGGTAGCTATGGTACTCCAGAA-3'
MCP-1	5'-CTGGATCGGAACCAAATGAG-3'	5'-TGAGGTGGTTGTGGAAAAGG-3'
IL-10	5'-ATCGATTTCTCCCCTGTGAA-3'	5'-TGTCAAATTCATTCATGGCCT-3'
Arginase-1	5'-CAGAAGAATGGAAGAGTCAG-3'	5'-CAGATATGCAGGGAGTCACC-3'
TGF- β	5'-GACCGCAACAACGCCATCTAT-3'	5'-GGCGTATCAGTGGGGGTCAG-3'
Ym-1	5'-CAGGTCTGGCAATTCTTCTGAA-3'	5'-GTCTTGCTCATGTGTGTAAGTGA-3'
Fizz-1	5'-TCCCAGTGAATACTGATGAGA-3'	5'-CCACTCTGGATCTCCCAAGA-3'
VEGF	5'-CTGTGCAGGCTGCTGTAACG-3'	5'-GTTCCCGAAACCCTGAGGAG-3'
Csf2ra	5'-AGACCCTCAGGAAGGACCTC-3'	5'-CGTCTATCAGCATCGCTTCA-3'
IRF5	5'-CAGGTGAACAGCTGCCAGTA-3'	5'-GGCCTTGAAGATGGTGTGT-3'
β -actin	5'-CTAAGGCCAACCGTGAAAAG-3'	5'-ACCAGAGGCATACAGGGACA-3'

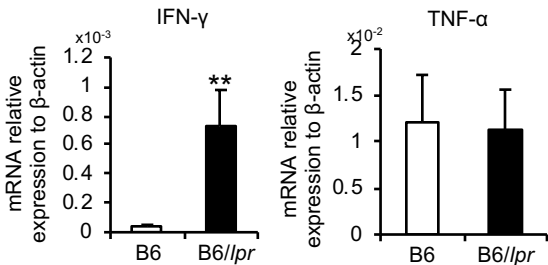
Supplementary Figure S1



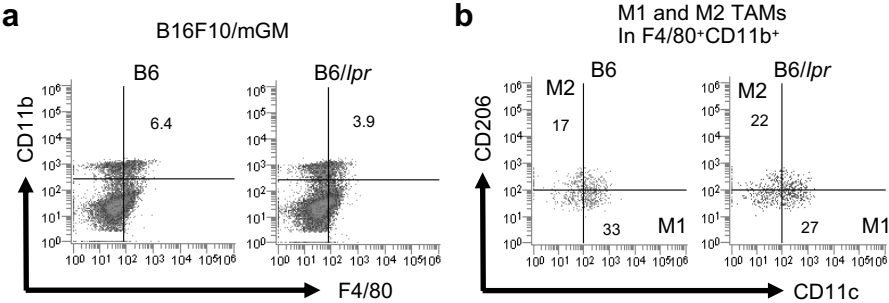
Supplementary Figure S2



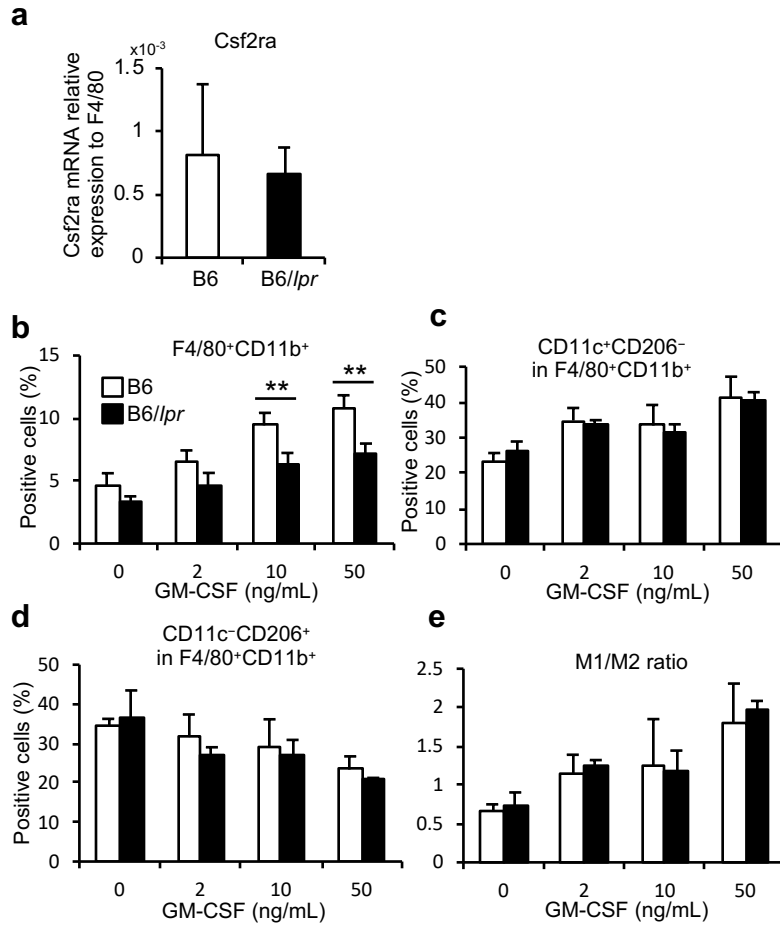
Supplementary Figure S3



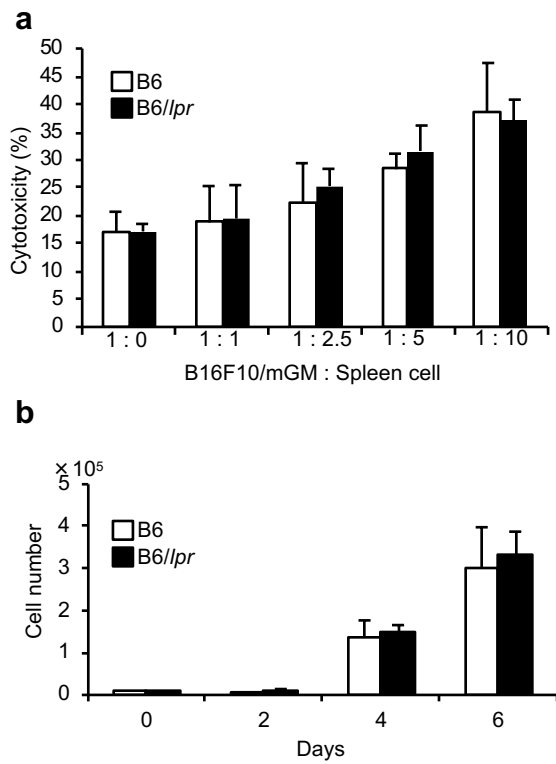
Supplementary Figure S4



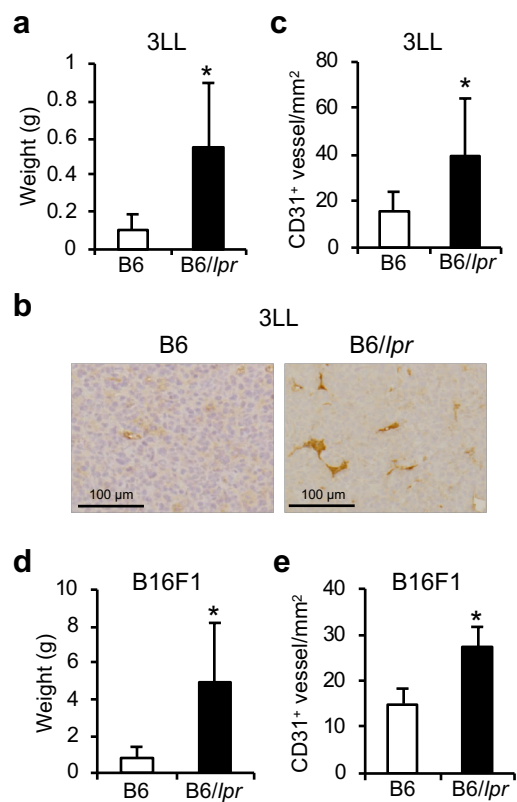
Supplementary Figure S5



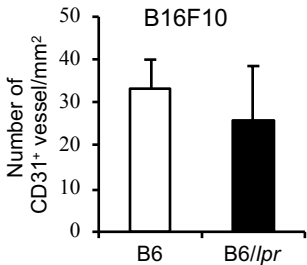
Supplementary Figure S6



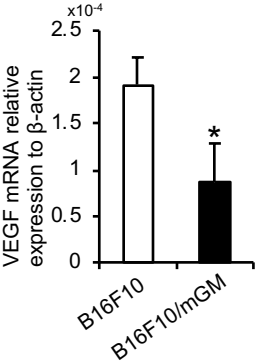
Supplementary Figure S7



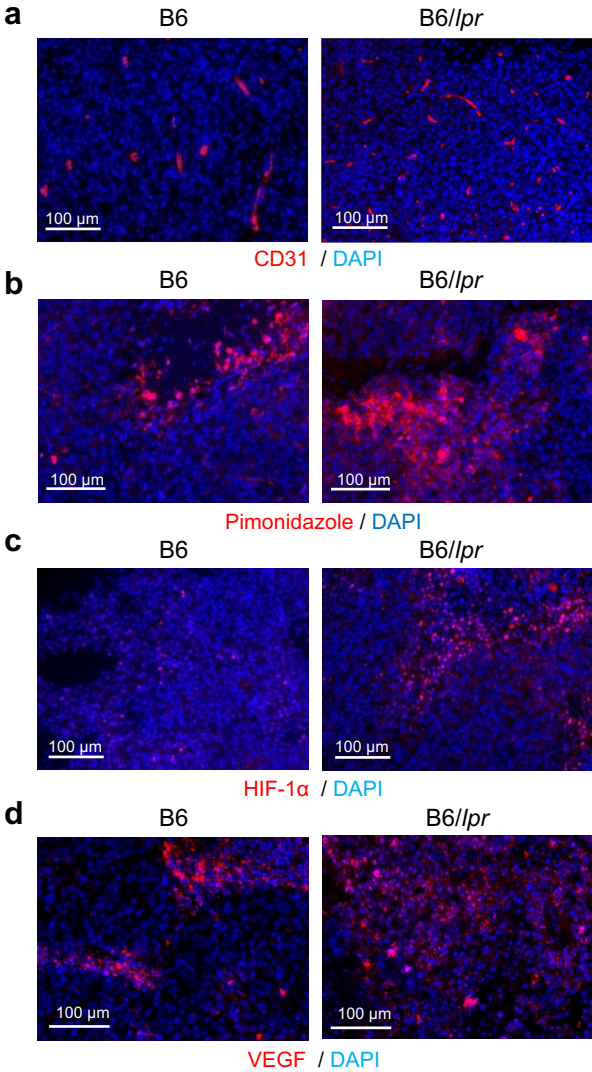
Supplementary Figure S8



Supplementary Figure S9



Supplementary Figure S10



Supplementary Figure S11

